Available online at www.sciencedirect.com
SCIENCE DIRECT®
Earth and Planetary Science Letters 236 (2005) 430–442
EPSL
www.elsevier.com/locate/epsl

# Fe isotope fractionation on FeS formation in ambient aqueous solution

Ian B. Butler [a,*], Corey Archer [b,1], Derek Vance [c], Anthony Oldroyd [a], David Rickard [a]

[a] School of Earth Ocean and Planetary Sciences, Cardiff University, Park Place, Cardiff, CF10 3YE, U.K.
[b] Department of Geology, Royal Holloway University of London, Egham, Surrey TW20 0EX, U.K.
[c] Department of Earth Sciences, University of Bristol, Wills Memorial Building, Queen's Road, Bristol, BS8 1RJ, U.K.

Received 3 November 2004; received in revised form 17 February 2005; accepted 6 May 2005
Available online 29 June 2005
Editor: B. Wood

**Abstract**

Iron sulfide phases are the ultimate repository of iron and reduced sulfur in sediments. The sulfur isotope geochemistry of pyrite has had much to tell us about modern and ancient Earth environments and it is likely that Fe isotopes will too, once fractionations for key processes are known. We report the results of an experimental study of Fe isotope fractionation on precipitation of FeS, synthetic mackinawite, from excess aqueous Fe(II) solutions by addition of sodium sulfide solution at 2–40 °C. The results show a significant kinetic isotope effect in the absence of a redox process. No detectable effect of temperature on the fractionation factor was observed. The Fe isotope fractionation for zero-age FeS is $\Delta_{Fe(II)-FeS} = 0.85 \pm 0.30‰$ across the temperature range studied, giving a kinetic isotope fractionation factor of $\alpha_{Fe(II)-FeS} = 1.0009 \pm 0.0003$. On ageing, the FeS in contact with aqueous Fe(II) becomes progressively isotopically heavier, indicating that the initial fractionations are kinetic rather than equilibrium. From published reaction mechanisms, the opportunity for Fe isotope fractionation appears to occur during inner sphere ligand exchange between hexaqua Fe(II) and aqueous sulfide complexes. Fe isotope fractionation on mackinawite formation is expected to be most significant under early diagenetic situations where a readily available reactive Fe source is available. Since $FeS_{(aq)}$ is a key reactive component in natural pyrite formation, kinetic Fe isotope fractionations will contribute to the Fe isotope signatures sequestered by pyrite, subject to the relative rate of $FeS_2$ formation versus $FeS–Fe(II)_{(aq)}$ isotopic equilibration.


*Keywords:* Fe isotopes; iron sulfide; mackinawite; pyrite; isotope fractionation; plasma source mass spectrometry

## 1. Introduction

Studies of the geochemical behaviour of the light stable isotopes of S, H, N, O and C have contributed greatly to our understanding of the inorganic

* Corresponding author. Tel.: +44 2920 875801; fax: +44 2920 874326.
*E-mail address:* Butler@earth.cf.ac.uk (I.B. Butler).
[1] Present address: Department of Earth Sciences, University of Bristol, Wills Memorial Building, Queen's Road, Bristol, BS8 1RJ, U.K.

0012-821X/$ - see front matter © 2005 Elsevier B.V. All rights reserved.
doi:10.1016/j.epsl.2005.05.022

and biological geochemistry of surficial or near surficial environments over the last 60 years [1–3]. Similarly, the comparatively recent advent of methods which readily permit the accurate and precise determination of Fe isotope fractionations presents geochemists with a new and potentially valuable tool with which to investigate the biogeochemistry of Fe in low temperature environments. Significant variation of iron isotope ratios, $^{56}Fe/^{54}Fe$ and $^{57}Fe/^{54}Fe$, have been reported from a number of natural systems [4–6], with a reported range in $^{56}Fe/^{54}Fe$ of ~4‰. The data suggest that Fe isotopes have great potential as probes to track biogeochemical processes in the natural environment. The experimental database for the mechanisms and magnitudes of individual iron isotope fractionation processes, which are necessary to interpret the natural data, is limited but growing [6]. In general it is the case that the greatest $^{56}Fe/^{54}Fe$ fractionations occur during both biologic (up to −1.7‰) and abiologic (up to 12‰) processes which involve partitioning of iron between the ferrous and ferric states [7–11]. Non-redox processes have been observed to produce smaller isotopic fractionations, typically up to 1‰ [11–14].

A number of studies have now been published that together show significant variation in the Fe isotope compositions of natural pyrite from a variety of geological environments. Hydrothermal sulfides from the Lucky Strike vent site (37°17′ N, Mid-Atlantic Ridge) show a $\delta^{57}Fe$ range of −3.16‰ to −1.62‰ (equivalent to $\delta^{56}Fe$ of −2.1‰ to −1.08‰) for pyrite and marcasite samples, and a $\delta^{57}Fe$ range of −0.70‰ to 0.51‰ (equivalent to $\delta^{56}Fe$ of −0.47‰ to 0.34‰) for chalcopyrite samples [15]. Pyrite and marcasite from low to medium temperature assemblages displayed isotopically lighter compositions compared to those from higher temperature assemblages. Pyrite from hydrothermally altered oceanic crust (Ocean Drilling Program site 801 C on the Pacific crust seaward of the Mariana Trench) showed $\delta^{57}Fe$ of −0.37‰ to −0.01‰ (equivalent to $\delta^{56}Fe$ of −0.25‰ to −0.01‰) [16], similar to, or slightly heavy isotope depleted than, Mid-Ocean Ridge Basalt [17]. Pyrite and chalcopyrite from the Grasberg Cu–Au deposit, Iryan Jaya, Indonesia display a $\delta^{57}Fe$ range of −3.02‰ to 1.62‰ (equivalent to $\delta^{56}Fe$ of −2.01‰ to 1.08‰) [18], and like the data for pyrite/marcasite and chalcopyrite from Lucky Strike, the Fe isotope composition ranges for the two minerals do not overlap. However, at Grasberg it is the pyrite which is enriched in the heavier isotope. These data are for sulfides formed in comparatively high temperature environments and, at the time of writing, data for pyrite formed in ambient sedimentary environments are sparse but have been measured for samples from a few Precambrian and Phanerozoic deposits. Pyrite nodules and ammonites from the upper Jurassic Kimmeridge formation of Dorset, U.K., show a $\delta^{57}Fe$ range of −0.31‰ to −0.45‰ (equivalent to a $\delta^{56}Fe$ range of −0.21‰ to −0.30‰) [19]. Pyrite from banded iron formations of the Transvaal Craton has a $\delta^{56}Fe$ range of −1.3‰ to −2.43‰ [20]. Rouxel et al. [21] present an extensive Fe isotopic dataset for diagenetic pyrite from sediments ranging in age from Archean to the Phanerozoic. These authors suggest that very negative Fe in sulfides prior to 2.3 Ga (down to −3.5‰ for $^{56}Fe$) are the result of precipitation from a reservoir in which heavy Fe has been depleted by iron oxide formation in the form of BIFS. The assumption is that diagenetic pyrite is a passive recorder of the Fe isotope composition of a reduced Fe reservoir that has been depleted of heavy Fe isotopes by oxide precipitation, but no experimental data exist for the magnitude of Fe isotope fractionations associated with iron sulfide formation. In this paper, we report an experimental investigation of the fractionation of Fe isotopes between dissolved and condensed phases during the fast precipitation of FeS from aqueous Fe(II) and S(−II). We examine the influence of ageing the precipitate in contact with excess $Fe(II)_{(aq)}$, of precipitation temperature and of mixing ratio on Fe isotope fractionation. We consider the results with reference to published reaction mechanisms for mackinawite formation as a first step in understanding the nature and extent of geologically important Fe isotope fractionations in the Fe–S system.

### 1.1. Reaction pathways in the Fe–S system

Iron is commonly fixed in sedimentary systems as iron sulfides, and iron sulfide formation is linked intimately with global biogeochemical cycles for Fe,

S, C, H and O. Under natural conditions where $Fe^{2+}_{(aq)}$ and $S(-II)_{(aq)}$ ion activity products exceed the $K_{sp}$ for FeS, the first precipitate is nanoparticulate iron(II) monosulfide. The net stoichiometry on reaction of Fe(II) with aqueous hydrogen sulfide or bisulfide is:

$$Fe^{2+}_{(aq)} + H_2S_{(aq)} = FeS_{(s)} + 2H^+_{(aq)} \quad (1)$$

$$Fe^{2+}_{(aq)} + HS^-_{(aq)} = FeS_{(s)} + 2H^+_{(aq)}. \quad (2)$$

There is no transformation of the redox state of the Fe or S on FeS formation. This material has been described previously as amorphous FeS. In fact, detailed kinetic studies [22] and structural analyses [23,24] show that this phase is tetragonal FeS, equivalent to the mineral mackinawite. The "amorphous" tag comes from the broad, low intensity powder XRD spectra. Wolthers et al. [24] showed that this feature derives mainly from the nanoparticuate size of the precipitates rather than from an amorphous structure.

In sedimentary systems, FeS has been often implicated as an intermediate phase in pyrite formation [25–29]. Detailed investigations of the kinetics and mechanism of pyrite formation reveal that there are two reaction paths that may be significant in natural systems, the polysulfide [30,31] and $H_2S$ [32,33] pathways. Other proposed reaction pathways can readily be explained in terms of either the polysulfide or $H_2S$ pathways [34]. Both the polysulfide and $H_2S$ pathways proceed via a dissolved iron sulfide intermediate which, based on voltammetric evidence, is an aqueous FeS cluster complex [33,35]. Thus the pathways may be written:

$$FeS_{(s)} \rightarrow FeS_{(aq)} \quad (3)$$

$$FeS_{(aq)} + Sn^{2-} = FeS_2 + S^{2-}_{n-1} \quad \text{Polysulfide pathway} \quad (4)$$

$$FeS_{(aq)} + H_2S = FeS_2 + H_2 \quad H_2S \text{ pathway}. \quad (5)$$

Thus, FeS is not directly converted to pyrite, rather FeS dissolves and pyrite forms or $FeS_{(aq)}$ is formed and reacts to form pyrite. The formation of $FeS_{(aq)}$ is an intermediate step during FeS precipitation [22] and pyrite formation. Fe isotope fractionation during FeS or $FeS_{(aq)}$ formation will contribute to the isotope signature of sedimentary pyrite from throughout the geological record.

## 2. Methods

### 2.1. FeS precipitation

All experimental reagents were of analytical grade and used without further purification. All acids used were of Suprapur™ grade. Solutions were prepared using 18.2 MΩ cm deionised water sparged with $O_2$-free grade nitrogen. All experimental reagents and products are oxygen sensitive and all experimental procedures (with the exception of precipitation at 2, 10 and 40 °C) were performed in an MBraun Labmaster 130 recirculating anoxic chamber with an $N_2$ atmosphere and $O_2 < 1$ ppmv. All experiments were performed as duplicates in separate reaction vessels. The Fe(II) source had a $\delta^{56}$Fe of +0.50‰ relative to IRMM.

Aqueous sulfide solution (2 or 10 ml of 0.05 M $Na_2S \cdot 9H_2O$) was injected into an excess aqueous Fe(II) solution (100 ml of 0.05 M $(NH_4)_2Fe(SO_4)_2 \cdot 5H_2O$) to precipitate FeS. Unless specified, 10 ml of sulfide was the standard volume added. The final pH of the reaction solution was $4.0 \pm 0.1$. After precipitation the product was collected by vacuum filtration on a 0.45 μm white cellulose nitrate membrane filter or a 0.02 μm Anodisc™ membrane filter. The filtrate solution containing the remaining dissolved Fe(II) was treated with excess 1 M sulfide solution to quantitatively precipitate the residual Fe. A 10 ml aliquot of this suspension was vacuum filtered to collect the precipitate. The solid products of the reaction were taken up in 10 M HCl.

For precipitation experiments at temperatures of 2, 10 and 40 °C, a Haake DC10/K10 circulator was used to maintain reaction temperature. Solutions were prepared in serum bottles with self-sealing rubber septa in the anoxic chamber. Reagents were brought to temperature outside the chamber, and sulfide was injected into the excess Fe using a hypodermic syringe. The serum bottles were returned to the anoxic chamber for filtration. For experiments in which FeS was allowed to age for up to 168 h in contact with the Fe(II) solution, serum

Table 1
Experimental conditions, fractionation factors and isotopic mass balance for FeS precipitation experiments

| Experiment | Experimental variable | FeS fraction[a] | Experimental results | | | | | | | Replicate analysis BCR-1 | |
|---|---|---|---|---|---|---|---|---|---|---|---|
| | | | $\delta^{56}$Fe FeS IRMM (‰) | $\delta^{57}$Fe FeS IRMM (‰) | $\delta^{56}$Fe Fe(II) IRMM (‰) | $\delta^{57}$Fe Fe(II) IRMM (‰) | ΔFe(II)-FeS ($^{56}$Fe)[b] (‰) | $\alpha'$(Fe(II)-FeS ($^{56}$Fe)[b] (‰) | $\delta^{56}$Fe mass balance | $\delta^{56}$Fe ‰ IRMM (‰) | $\delta^{57}$Fe ‰ IRMM (‰) |
| A-Fe-0-A | Aged 0 h | 0.1 | −0.25 | −0.28 | 0.97 | 1.43 | 1.22 | 1.0012 | 0.35 | 0.19 | 0.33 |
| A-Fe-0-B | Aged 0 h | 0.1 | −0.18 | −0.30 | 0.81 | 1.33 | 0.99 | 1.0010 | 0.22 | 0.15 | 0.24 |
| A-Fe-24-A | Aged 24 h | 0.1 | −0.15 | −0.15 | 0.66 | 1.03 | 0.81 | 1.0008 | 0.09 | 0.09 | 0.16 |
| A-Fe-24-B | Aged 24 h | 0.1 | −0.07 | −0.20 | 0.72 | 1.19 | 0.79 | 1.0008 | 0.14 | 0.16 | 0.25 |
| A-Fe-48-A | Aged 48 h | 0.1 | 0.00 | 0.00 | 0.58 | 0.82 | 0.58 | 1.0006 | 0.02 | 0.19 | 0.31 |
| A-Fe-48-B | Aged 48 h | 0.1 | 0.06 | 0.12 | 0.44 | 0.62 | 0.38 | 1.0004 | −0.10 | 0.12 | 0.21 |
| A-Fe-168-A | Aged 168 h | 0.1 | 0.21 | 0.42 | 0.53 | 0.84 | 0.32 | 1.0003 | 0.00 | 0.12 | 0.17 |
| A-Fe-168-B | Aged 168 h | 0.1 | 0.21 | 0.23 | 0.56 | 0.75 | 0.35 | 1.0003 | 0.02 | 0.09 | 0.18 |
| F-Fe-0.02-A | 0.02 (μm) filter | 0.1 | −0.09 | −0.24 | 0.41 | 0.62 | 0.50 | 1.0005 | −0.14 | 0.08 | 0.10 |
| F-Fe-0.02-B | 0.02 (μm) filter | 0.1 | −0.27 | −0.39 | 0.49 | 0.74 | 0.76 | 1.0008 | −0.09 | 0.10 | 0.15 |
| R-Fe-2-A | 2 (ml) S(−II) | 0.02 | 0.17 | 0.18 | 0.47 | 0.74 | 0.30 | 1.0003 | −0.03 | 0.10 | 0.19 |
| R-Fe-2-B | 2 (ml) S(−II) | 0.02 | 0.20 | 0.30 | 0.58 | 0.93 | 0.38 | 1.0004 | 0.07 | 0.13 | 0.19 |
| T-Fe-2-A | Temp 2 °C | 0.1 | −0.43 | −0.40 | 0.70 | 1.06 | 1.13 | 1.0011 | 0.09 | 0.08 | 0.19 |
| T-Fe-2-B | Temp 2 °C | 0.1 | −0.38 | −0.70 | 0.60 | 0.76 | 0.98 | 1.0010 | 0.01 | 0.12 | 0.20 |
| T-Fe-10-A | Temp 10 °C | 0.1 | −0.48 | −0.67 | 0.50 | 0.78 | 0.98 | 1.0010 | −0.10 | 0.11 | 0.23 |
| T-Fe-10-B | Temp 10 °C | 0.1 | −0.45 | −0.81 | 0.54 | 0.92 | 0.99 | 1.0010 | −0.05 | 0.10 | 0.15 |
| T-Fe-40-A | Temp 40 °C | 0.1 | −0.36 | −0.57 | 0.69 | 0.96 | 1.05 | 1.0011 | 0.09 | 0.06 | 0.23 |
| T-Fe-40-B | Temp 40 °C | 0.1 | −0.31 | −0.33 | 0.66 | 0.98 | 0.97 | 1.0010 | 0.07 | 0.12 | 0.22 |
| Total $\delta^{56}$Fe mass balance | | | | | | | | | 0.03 ± 0.12 | | |

Calculation methods for fractionations, fractionation factors and mass balances are detailed in Section 3. Replicate analyses of USGS standard basalt BCR-1 are also tabulated. Analytical precision is $\delta^{56}$ Fe = ± 0.07‰ and $\delta^{57}$ Fe = ± 0.11‰ at the 2$\sigma$ level.

[a] Fe atom ratio between precipitated FeS and the initial Fe(II) solution.

[b] Fractionation factors are calculated based on $\delta^{56}$ Fe data.

bottles were agitated continuously on a shaking platform. Experimental series and variables are summarized in Table 1.

### 2.2. Isotopic analysis

All Fe isotopic measurements of FeS precipitates were performed on a GV Micromass instrument at Royal Holloway, University of London. A small aliquot of the samples from the experiments, in 10 M HCl, was evaporated to dryness and re-dissolved in twice-distilled 2% (v/v) $HNO_3$ for introduction to the mass spectrometer.

The two key analytical challenges with Fe isotopic measurement by multi-collector inductively-coupled plasma mass spectrometry (MC-ICPMS) are: 1) reducing spectral interferences on Fe isotopes ($^{14}N^{40}Ar$ on $^{54}Fe$, $^{16}O^{40}Ar$ on $^{56}Fe$ and $^{16}O^{1}H^{40}Ar$ on $^{57}Fe$); 2) the correction for instrumental mass discrimination. For the analysis of these large samples, the impact of the argide molecular interferences was minimised by reducing the source extract potential and by running concentrated sample solutions (3–6 ppm), thus maximising the signal to noise ratio. Typical ion beams for 3–6 ppm solutions of both standards and samples were $5\times10^{-11}$A for $^{56}Fe$, $\sim0.3\times10^{-11}$A for $^{54}Fe$ and $\sim0.12\times10^{-11}$A for $^{57}Fe$. Typical backgrounds, measured on 2% $HNO_3$ prior to each sample analysis, were $0.1–0.3\times10^{-14}$A for $^{56}Fe$, $0.1–0.5\times10^{-15}$A for $^{54}Fe$ and up to $0.5\times10^{-15}$A for $^{57}Fe$. Thus, in all cases, the background constituted ≤0.25‰ of the Fe signal. These backgrounds were subtracted from sample beams so that their contribution to analytical uncertainty is trivial.

Correction for instrumental mass discrimination was achieved by standard-bracketing. The typical drift in standard analyses during an entire 10-h analytical session was 0.5–1.5‰, with shifts between standards either side of samples being ≤0.1‰. Mass discrimination, as monitored by a pure standard, need not be appropriate for Fe separated from a mineral or rock matrix [36]. We have assessed this potential problem using repeated measurements of USGS rock standard BCR-1 (Table 1). Each basalt analysis represents a separate digestion of powder from which Fe was separated using now standard techniques [37]. BCR-1 gives a $\delta^{56}Fe_{IRMM}$ of $+0.12\pm0.07$‰ ($n=17$) where $\delta^{56}Fe_{IRMM}$ is defined as:

$$\delta^{56}Fe_{IRMM} = \left(\left(\delta^{56}Fe_{sample} - \delta^{56}Fe_{IRMM}\right)/\delta^{56}Fe_{IRMM}\right)\times 1000. \quad (6)$$

The quoted uncertainty, in common with all those cited here, is $2\sigma$. The value obtained for BCR-1 is

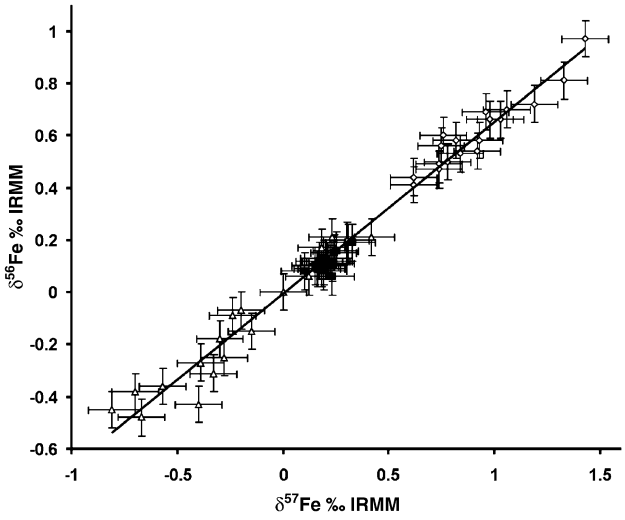


Fig. 1. Analytical quality control data using $\delta^{56}Fe$ and $\delta^{57}Fe$ for FeS precipitates (open triangles), Fe(II) solutions (open diamonds) and basalt standard BCR-1 (filled squares). The tight fit of the line (MSWD = 1.05) indicates that unaccounted for residual spectral interferences are absent. The slope of the line ($1.535\pm0.062$) is consistent with the mass differences between the two isotope ratios.

identical to that for this and other basalts reported by Beard et al. [17]. Our analytical uncertainties, 0.07‰ for $\delta^{56}$Fe and 0.11‰ for $\delta^{57}$Fe, are based on these replicate analyses of BCR-1. The average deviation of replicate analyses from their mean (for the 18 replicate isotope measurements in Table 1) is 0.04‰ for $\delta^{56}$Fe (range is 0–0.09‰) and 0.08‰ for $\delta^{57}$Fe (range is 0.02–0.15‰).

Of course, silicate rock matrices are also very different from those involved here. Two further arguments increase our confidence in the lack of matrix effects in our data. Firstly, mass scans in the range 20–36 amu revealed only very small impurities in our sample solutions relative to blank 2% $HNO_3$. Secondly, we passed aliquots of some test samples through our anion exchange column and compared the resulting $\delta^{56}$Fe with those for untreated samples. Three test samples on which we performed this procedure gave differences in $\delta^{56}$Fe between treated and untreated samples of 0.01‰, 0.13‰ and 0.16‰.

All the data from this study, as well as the BCR-1 data, are plotted in Fig. 1 as a $\delta^{56}$Fe vs $\delta^{57}$Fe plot. The tight fit of the line (MSWD = 1.05) confirms the absence of unaccounted-for residual spectral interferences and the slope of the line ($1.535 \pm 0.062$) is as expected from the mass differences between the two isotope ratios.

## 3. Results

Experimental conditions, isotopic analyses and fractionation factors are summarized in Table 1. Fractionations between the aqueous Fe(II) residue and mackinawite (FeS) are presented as $\Delta_{\mathrm{Fe(II)–FeS}}$, where

$$\Delta_{\mathrm{Fe(II)-FeS}} = \delta^{56}\mathrm{Fe}_{\mathrm{Fe(II)}} - \delta^{56}\mathrm{Fe}_{\mathrm{FeS}}. \quad (7)$$

The isotope fractionation factor, $\alpha'_{\mathrm{FeS–Fe(II)}}$ is defined by:

$$\alpha'_{\mathrm{Fe(II)-FeS}} = (\delta^{56}\mathrm{Fe}_{\mathrm{Fe(II)}} + 1000) / (\delta^{56}\mathrm{Fe}_{\mathrm{FeS}} + 1000). \quad (8)$$

The mass balance is the weighted sum of the isotopic composition of the precipitate and residue. Here we present the isotopic mass balance relative to the Fe isotopic composition of the ammonium ferrous sulfate reactant, which has a composition of $\delta^{56}$Fe = 0.50‰ IRMM.

$$0 = (f\delta^{56}\mathrm{Fe}_{\mathrm{Fe(II)}} + (1-f)\delta^{56}\mathrm{Fe}_{\mathrm{FeS}}) - 0.5 \quad (9)$$

where $f$ is the fraction of the total Fe (total Fe has $\delta^{56}$Fe = 0.50‰) which remains as aqueous Fe(II). In this case, a perfect mass balance will be equal to zero. A scatter plot of the calculated isotopic mass balance compared to the ideal theoretical mass balance for each experimental replicate is shown in Fig. 2.

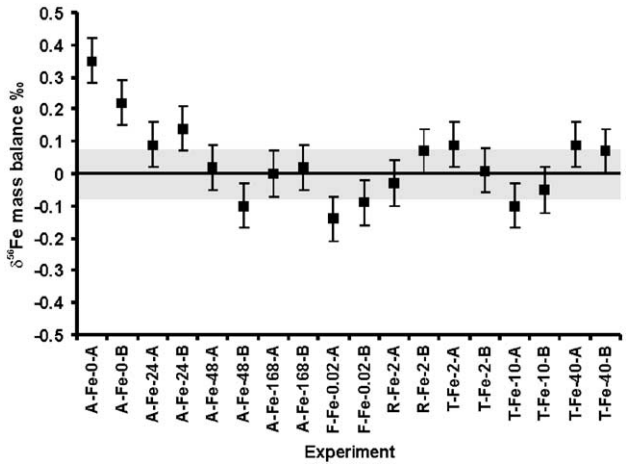


Fig. 2. $\delta^{56}$Fe isotopic mass balance scatter plot. The isotopic mass balance for each experimental replicate is calculated from the measured isotopic composition of the FeS and $Fe(II)_{(aq)}$ reservoirs using Eq. (9). The grey band illustrates analytical uncertainty either side of the theoretical ideal mass balance.

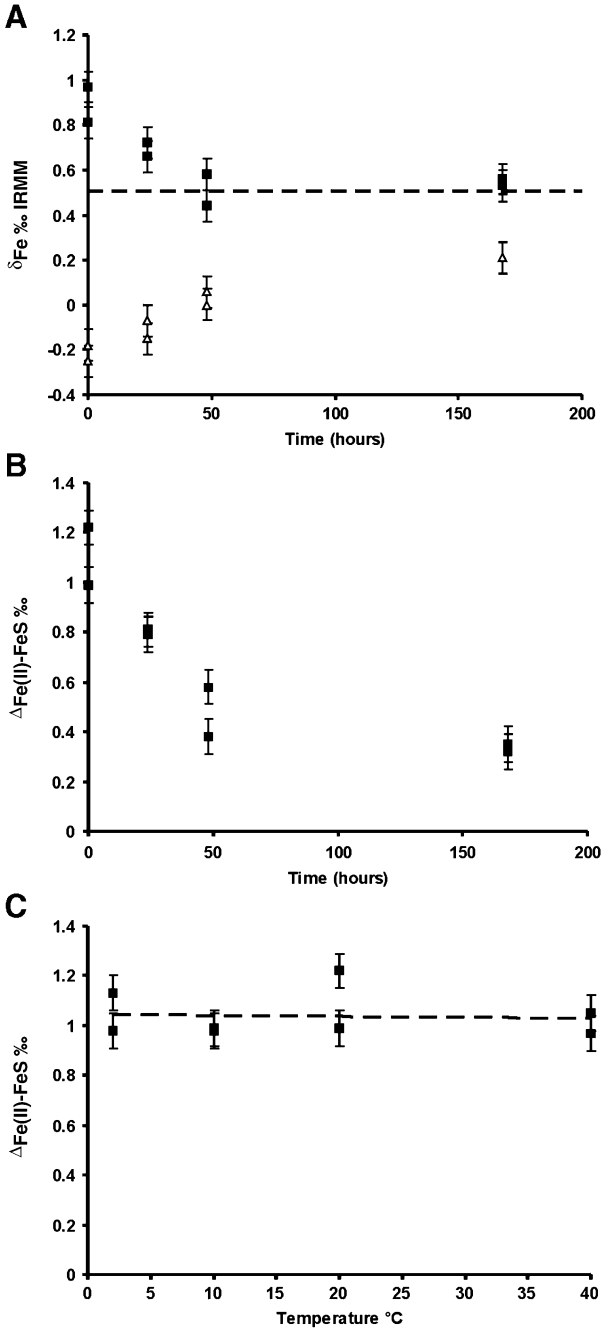


Fig. 3. (A) Progressive change in $\delta^{56}$Fe for both $FeS_{(s)}$ (open triangles) and $Fe(II)_{(aq)}$ (filled squares) on ageing of the precipitated FeS in contact with $Fe(II)_{(aq)}$. $FeS_{(s)}$ represents 10% of the total Fe present in the system. After 48 h the isotopic composition of $Fe(II)_{(aq)}$ appears unchanging. However, it is the smallest isotopic reservoir which reveals changes in the system, and the $\delta^{56}$Fe composition of FeS is apparently still changing after 168 h. (B) Change in $\Delta_{Fe(II)-FeS}$ on ageing of FeS in contact with the aqueous Fe isotope reservoir at 20 °C. FeS becomes progressively less isotopically light relative to the Fe(II) source, consistent with the measured fractionations being kinetic in origin. Curvature suggests that $\Delta_{Fe(II)-FeS}$ is asymptotic towards a metastable disequilibrium fractionation. (C) Effect of precipitation temperature on the Fe isotope fractionation on FeS precipitation. Kinetic fractionations on FeS precipitation are temperature independent in the range 2–40 °C, within the errors of the present study.

In all cases, the FeS product was isotopically light compared to its aqueous counterpart. On ageing FeS in contact with the residual aqueous solution $\delta^{56}Fe_{FeS}$ increases with time and $\delta^{56}Fe_{Fe(II)}$ decreases with time (Fig. 3A). Fractionation factors progressively decrease with time from 0 to 168 h (Fig. 3B) and the precipitate becomes isotopically heavier, but remains light compared to the coexisting aqueous Fe(II) reservoir. Within experimental error we observe no measurable effect of temperature on Fe isotope fractionation on the precipitation of FeS in the range 2–40 °C (Fig. 3C). The Fe isotope fractionation for all zero-age FeS precipitates between 2–40 °C ($n=12$) is $\Delta_{Fe(II)-FeS}=0.85\pm0.30$, yielding an isotope fractionation factor in the same temperature range of $\alpha'_{Fe(II)-FeS}=1.0009\pm0.0003$. Experiments using a larger Fe excess (50:1) and a smaller filter size (0.02 μm) for collection of the mackinawite showed somewhat heavier isotopic signatures ($\Delta_{Fe(II)-FeS}=0.34‰$ ($n=2$) and 0.63‰ ($n=2$), respectively) than did other zero age FeS precipitates.

## 4. Discussion

On ageing the FeS precipitate, Fe isotope fractionations progressively decrease and the $\delta^{56}Fe$ composition in FeS becomes heavier, from $\Delta_{Fe(II)-FeS}=0.85‰\pm0.30$ for zero-age FeS to $\Delta_{Fe(II)-FeS}=0.34‰$ after 168 h. FeS is a moderately insoluble salt ($pK_{sp}=3.00$; [38]) and we interpret this trend as the slow progression from an initial kinetic isotope fractionation towards an isotopic steady state condition. We consider that a dissolution–reprecipitation is the most likely mechanism for isotope exchange between the two reservoirs during ageing. Böttcher et al., [39] report a similar kinetic effect for S isotope fractionation on FeS precipitation. Hence fractionation factors, $\alpha'$, are termed kinetic fractionation factors to distinguish them from the equilibrium fractionation factor, $\alpha$. Both are defined by Eq. (8), but $\alpha$ is applicable only where isotope exchange at chemical equilibrium is established. Although the curvature of the ageing trend in Fig. 3B is suggestive of an approach towards a steady state isotopic composition, there is insufficient evidence to confirm that a persistent steady state is attained in the present experimentation. In Fig. 3A we show the evolution of isotopic composition of the FeS and Fe(II) isotopic reservoirs versus time. The curve for $\delta^{56}Fe_{Fe(II)}$ versus time apparently indicates a steady state composition for this reservoir after 48 h. However, the Fe(II) reservoir represents 90% of the total Fe in the system and is a considerably less sensitive indicator of changes in the system than the isotopic composition of the FeS, which represents 10% of the total Fe. The $\delta^{56}Fe_{FeS}$ versus time curve for FeS indicates that the system is still changing over 48–168 h. Even if the system was at steady state, isotopic exchange occurs between Fe(II) in solution and the FeS nanoparticle surface but not between the Fe(II) in solution and the bulk FeS. As a consequence, it is likely that apparent steady state isotopic compositions might represent metastable disequilibrium fractionations, and not true equilibrium fractionations. The fractionation between aqueous Fe(II) and FeS is expected to change slowly as Ostwald ripening of the precipitated FeS progresses.

Equilibrium isotope fractionations typically show a dependence on $1/T$ or $1/T^2$ [1]. Similarly, unidirectional and incomplete processes where kinetic isotope fractionation is dominant often show a temperature dependence since the respective rate constants for the reaction of light and heavy isotopes are also temperature dependent [40]. However, for FeS formation in the range 2–40 °C, any relationship between fractionation factor and temperature falls within the range of experimental and analytical error of this study. We note that it is often the case that kinetic isotope fractionations are less temperature sensitive than are equilibrium fractionations for the same chemical system. Consequently, the kinetic fractionation factors presented here appear to be applicable to FeS formation at all ambient Earth surface temperatures.

### 4.1. Fractionation and reaction mechanism

The mechanism of FeS formation in aqueous solutions at low temperatures involves two competing reactions with aqueous $H_2S$ and $HS^-$ [22]. The rate laws for both reactions are consistent with Eigen–Wilkins mechanisms [41] in which the rate is determined by the exchange between water and sulfide molecules in hexaqua iron(II) sulfide outer sphere complexes $Fe(H_2O)_6^{2+}\cdot H_2S_{(aq)}$ and $Fe(H_2O)_6^{2+}\cdot HS^-_{(aq)}$ and the inner sphere complexes, $FeH_2S\cdot(H_2O)^{2+}_{5(aq)}$ and

$Fe(HS) \cdot (H_2O)^{5+}_{(aq)}$. The subsequent nucleation of FeS is fast. There is no observable lag phase and it is probable that aqueous FeS clusters, $FeS_{aq}$, with structures similar to the fundamental structural elements in mackinawite, are involved [35].

The first dissociation constant for $H_2S$, $pK_{1H2S}$ is 6.98 [42] and both pathways may be active in near pH neutral environments [22]. Experimentally we injected 0.05 M $Na_2S \cdot 9H_2O$, effectively a 0.05 M NaOH solution, into a 0.05 M Fe(II) solution. The high pH of the sulfide solution and the fact that pH neutralization occurs only after the release of protons on FeS formation (Eqs. (1) and (2)) means that the present experimentation is dominated by the bisulfide pathway. Using published kinetics [22], initial rates of Fe removal from solution by the bisulfide pathway approach $3 \times 10^2$ mol $l^{-1}$ $s^{-1}$ in this study, and FeS precipitation is experimentally instantaneous.

In the reactant Fe(II) solution, Fe speciation is dominated by hexaqua Fe(II), but with up to 90% of the Fe(II) existing as an $FeSO^0_{4(aq)}$ ion pair (calculated using MINEQL+ v4.5, Environmental Research Software, Hallowell, ME, USA). This ion pair is a weak outer-sphere complex with hexaqua Fe(II) and ligand exchange of sulfide with water still controls the reaction rate during FeS formation. Both FeS forming reaction mechanisms proceed via the exchange of $H_2O$ with either $H_2S$ or $HS^-$ followed by the release of protons after the formation of a charged inner sphere complex [22]. Upon further condensation there is no mechanism to break and make bonds and physically separate Fe isotopes, and for this reason we propose that isotopic fractionation occurs during inner-sphere ligand exchange, during the formation of $FeS_{aq}$, and before development of the condensed phase. The effect, if any, of the formation of outer sphere $FeSO_{4(aq)}$ ion pairs on the extent of Fe isotope fractionation is impossible to assess from the present data, but may be insignificant since the Fe(II) nucleus is not involved in the substitution reaction. FeS precipitates with an isotopically light Fe composition and the progression towards a heavier composition on ageing in contact with aqueous Fe(II) are consistent with kinetic isotope fractionation processes. During ligand exchange, isotopically lighter Fe participates in reactions at a faster rate than does heavier Fe and the light isotope is preferentially partitioned into both $FeS_{(aq)}$ and ultimately into $FeS_{(s)}$. Our suggestion that Fe isotope fractionation is likely to occur during ligand exchange is broadly consistent with the results of Schauble et al. [43] who calculated theoretical equilibrium isotope fractionation factors for a number of pairs of inner-sphere Fe complexes in aqueous solution.

We have considered whether Fe sorption on FeS surfaces contributes to the fractionation observed. Wolthers et al. [44] used potentiometric titrations to determine the pH at which the FeS surface has a zero proton charge ($pH_{PZC}$) and determined that, for freshly precipitated FeS, the $pH_{PZC}$ is ~7.5 and that the surface becomes increasingly positively charged at lower pH until saturated at pH ~6.5. At the final experimental pH of this investigation ($pH = 4 \pm 0.1$), the FeS surface is saturated and positive. Furthermore, dummy experiments show that Fe reacts with sulfide in a 1:1 ratio, suggesting that the extent of Fe uptake to the solid phase by sorption is insignificant compared to the extent of uptake by precipitation.

### 4.2. Comparison with other metal-sulfide systems

To date, the only other metal-sulfide isotope fractionation process that has been examined experimentally is the formation of CuS from aqueous Cu(II) and S(−II) [45]. In this case, $\Delta^{65}Cu_{Cu(II)–CuS}$ of 2.7–3.5‰ were recorded between 2 and 40 °C using an essentially identical experimental method to that described here. In contrast, precipitation of FeS results in $\Delta^{56}Fe_{Fe(II)–FeS}$ of $<1.1$‰ within the same temperature range. The effect of ageing the precipitate with the aqueous metal reservoir is more pronounced for FeS than was reported for CuS.

During FeS precipitation, aqueous Fe(II) is partitioned into the condensed phase via $FeS_{(aq)}$ clusters but remains as Fe(II). During CuS formation aqueous Cu(II) reacts with sulfide to form $Cu_3S_3$ rings which condense to $Cu_4S_5$ and $Cu_4S_6$ clusters [46] which are structurally similar to the condensed phase. During condensation Cu(II) is reduced to Cu(I) and the covellite product is a Cu(I) sulfide [46]. Cu(II) is released during condensation of $Cu_3S_3$ to $Cu_4S_5$ and $Cu_4S_6$ [46] and it is proposed that Cu isotope fractionation occurs during reduction of Cu(II) to Cu(I) with Cu(II) release providing the means of physically separating light and heavy isotopes [45,47]. On ageing of CuS and FeS in contact with their aqueous

isotopic reservoirs, the progress of isotopic equilibration is considerably faster for FeS than for CuS [45]. CuS is considerably less soluble than is FeS ($pK_{sp,FeS}=3.00$; [38]. $pK_{sp,CuS}=22.2$; [48]) which may limit mass exchange and progression towards isotopic steady state.

FeS is the only metal sulfide for which metal and sulfur isotope fractionation on precipitation has been determined. Böttcher et al. [39] showed that kinetic S isotope fractionations on FeS precipitation were $\alpha'_{MeS-HS^-}=0.9988\pm0.0007$ at 20 °C using a similar method to that employed herein. The kinetic isotope fractionation factor for Fe isotope fractionation on FeS formation between 2 and 40 °C is $\alpha'_{Fe(II)-FeS}=1.0009\pm0.0003$. For direct comparison with the data of Böttcher et al. [39], $\alpha'_{Fe(II)-FeS}$ is recalculated as $\alpha'_{FeS-Fe(II)}=0.9992\pm0.0003$. The fractionation factor for Fe is less than that for S isotope fractionation, but acts in the same direction and light isotopes are partitioned into the zero-age precipitate. For the S isotope system, abiogenic fractionation factors are small compared to those associated with microbial reactions [39], and do not contribute significantly to the isotopic composition of natural materials. In contrast, biological redox processes result in Fe isotope fractionations typically in the range of 1.3–1.5‰, enriching the Fe(III) phase with the heavy isotope [4,5]. Biological redox fractionations are often smaller than those recorded for inorganic redox processes partitioning Fe(II) and Fe(III). For example, kinetic isotope fractionations >10‰ have been recorded for the acid decomposition of iron bipyridyl complexes [8] and the equilibrium isotope fractionation between hexaqua Fe(III) and Fe(II) is of the order of 3‰ [9]. The kinetic isotope fractionation on FeS formation is of a similar order to those attained in biological systems, and in non-redox inorganic processes involving Fe(III) [4,5]. In contrast to the S isotope system, both inorganic and biological processes producing Fe isotope fractionations are expected to contribute to Fe isotope signatures of natural materials.

### 4.3. Application to natural systems

The FeS precipitated in our experiments is the synthetic equivalent of the mineral mackinawite and the experimental results can be considered in terms of mackinawite formation in natural systems. At the total sulfide concentrations of our experiments, the bisulfide pathway dominates. The importance of the two reactions for mackinawite formation is dependent on the total sulfide concentration and pH [22]. At 0.1 mM total sulfide, the bisulfide pathway dominates at pH>6.25 and is also likely to be the principal mechanism for mackinawite formation in most anoxic sedimentary environments. The reaction pathways are mechanistically uniform across the activity range from our experimental series to that of natural solutions [22]. In natural surface waters, Fe(II) speciation is dominated by hexaqua Fe(II), although the $FeSO_4^\circ$ ion pair may be significant [49], as it is in our experimentation. Thus, the Fe isotope fractionations presented herein are expected to be representative of those which may be attained in natural systems. For significant Fe isotope fractionation to be apparent, it is essential that a significant proportion of the Fe(II) reservoir remains as $Fe(II)_{(aq)}$ during the precipitation process, i.e. reservoir utilization must not proceed to completion. Thus Fe isotope fractionation on mackinawite formation may be recorded from situations (i) where total aqueous Fe(II) and S(−II) activities are low and of a similar magnitude and (ii) where aqueous Fe(II) activities are significantly greater than S(−II) activities. In many sedimentary environments, such situations may be represented by early diagenetic conditions near the suboxic–anoxic interface where sources of reactive, soluble, Fe outstrip sources of free sulfide from sulfate reduction [50,51]. However, investigations of methane-driven sulfate reduction of sediments from Black Sea environments [52,53], show an excess of reactive iron in deep limnic deposits which lie below the sulfate reduction maxima. In these conditions $H_2S$ is drawn down to a sulfidisation front where it reacts with Fe(III) and $Fe^{2+}$ which diffuses up from below. In such circumstances Fe isotope fractionations may be recorded from FeS formation deep below the suboxic–anoxic boundary.

In the global biogeochemical iron and sulfur cycles, iron and sulfur are ultimately sequestered in sediments as pyrite, and so Fe isotope ratios of ancient sedimentary pyrites provide a potential probe into palaeoenvironments. Kinetic Fe isotope fractionation on mackinawite formation will contribute to the total isotope Fe isotope fractionation recorded in the form of pyrite in the geological record. The extent of this contribution is subject to a number of factors inclu-

ding the Fe(II):S(−II) ratio during FeS formation, the relative rates of mackinawite and pyrite formation and the $FeS_{(aq)}$-pyrite isotope fractionation factor. Where pyrite formation is sufficiently rapid, incorporation of Fe from $FeS_{(aq)}$ or from mackinawite into pyrite (via mackinawite dissolution to form $FeS_{(aq)}$) may occur sufficiently fast to ensure that Fe showing the maximum kinetic isotope fractionation is fixed as pyrite. In cases where pyrite formation is slow then mackinawite may have time to establish an isotopic steady state with its aqueous Fe(II) reservoir and smaller kinetic Fe isotope fractionations will be transferred to pyrite. The extremely low solubility of pyrite in ambient aqueous systems means that incorporation of Fe into pyrite is a unidirectional process. This is a possible explanation for the disparity between published Fe isotope compositions for natural Phanerozoic sedimentary pyrite, which show $^{56}$Fe depleted compositions [20,21] and calculated equilibrium isotope fractionation factors, which predict $^{56}$Fe enriched pyrite compositions [54]. Further experimental work is required to establish the nature and extent of Fe isotope fractionation on pyrite formation. This work is required in order to ascertain whether pyrite is a passive recorder of the bulk isotopic composition of the Fe reservoir from which it is formed or whether the Fe isotope signature of the reservoir is modified significantly during fixation as pyrite.

The present contribution provides fundamental data for Fe isotope fractionation on the precipitation of mackinawite from aqueous Fe(II) solutions. Although in sedimentary systems the principle source of Fe in FeS is likely to be Fe(II) formed by bacterial reduction of Fe(III) oxyhydroxides, it is also possible that mackinawite may form via the sulfidation of solid Fe (III) oxyhydroxides such as goethite. The kinetics and mechanism of the sulfidation of goethite has been investigated by Rickard [55] and by Pyzik and Sommer [56], and these authors show that the reaction proceeds by dissolution of goethite and subsequent precipitation of mackinawite. Pyzik and Sommer [56] suggest that Fe(III) is reduced at the goethite surface by bisulfide species, to produce Fe(II) hydroxide and sulfur. Subsequent dissolution of the Fe(II) hydroxide is followed by mackinawite precipitation via the pathways described for an Fe(II) reactant [22]. Thus the sulfidation of goethite (and other Fe hydroxides and oxyhydroxides) is expected to produce maximum kinetic Fe isotope fractionations similar to those reported here. However, the extent of any additional Fe isotope fractionation related to Fe(III) reduction by sulfide on the goethite surface is unknown. The two experiments in the literature involving the inorganic dissolution of hematite by HCl [13] and goethite by the siderophore desferrioxamine mesylate [11] produced aqueous Fe(II) that was isotopically indistinguishable from the starting solid Fe(III). Congruent dissolution of an isotopically homogenous mineral surface transfers all the Fe from the surface layer dissolved into solution, and no fractionation is observed [6].

## 5. Conclusions

Kinetic Fe isotope fractionations, $\Delta_{Fe(II)–FeS} = 0.85 \pm 0.30‰$, occur on the formation of mackinawite by addition of aqueous sulfide to excess Fe(II) solution. The isotope effect is not related to any redox process in this system. The condensed phase Fe(II) is isotopically light relative to its aqueous counterpart. In the temperature range between 2 and 40 °C, there is no discernable effect of temperature on isotopic fractionation. However, on ageing of the FeS precipitate in contact with the aqueous Fe(II) residue the solid phase becomes progressively less depleted, consistent with the recorded maximum fractionations being kinetic in origin. Isotopic equilibrium cannot be shown to be established in the present experimentation, although the data indicate that at equilibrium $\Delta_{Fe(II)–FeS} < 0.3‰$. Comparison of the results with published mechanistic interpretations of mackinawite precipitation suggest that the opportunity for isotopic fractionation occurs during inner sphere exchange of sulfide and water ligands, with isotopically light Fe reacting fastest and becoming enriched in the condensed phase. Since $FeS_{(aq)}$ is a key reactive component in natural pyrite formation, kinetic Fe isotope fractionations will contribute to the Fe isotope signatures sequestered by pyrite, subject to the relative rates of $FeS_2$ formation and $FeS–Fe(II)_{(aq)}$ isotopic equilibration.

## Acknowledgements

We acknowledge financial support from the NERC (long term grant NER/L/S/2000/00611). The NERC

and Royal Holloway provided support for CA and for the establishment and maintenance of the Isoprobe facility at RHUL. We acknowledge the constructive reviews by Helen Williams, Clarke Johnson and two anonymous reviewers.

## References

[1] H.C. Urey, The thermodynamic properties of isotopic substances, J. Chem. Soc. 1947 (1947) 562.
[2] M. Schidlowski, J.M. Hayes, I.R. Kaplan, Isotopic inferences of ancient biochemistries: carbon, sulfur, hydrogen and nitrogen, in: J.W. Schopf (Ed.), Earth's Earliest Biosphere: Its Origin and Evolution, Princeton University Press, Princeton, 1983, pp. 149–186.
[3] J.M. Hayes, Fractionation of carbon and hydrogen isotopes in biosynthetic processes, in: J.W. Valley, D. Cole (Eds.), Stable Isotope Geochemistry, Reviews in Mineralogy and Geochemistry, vol. 43, Mineralogical Society of America, Washington, D.C., 2001, pp. 225–273.
[4] A.D. Anbar, Iron stable isotopes: beyond biosignatures, Earth Planet. Sci. Lett. 217 (2004) 223–236.
[5] B.L. Beard, C.M. Johnson, Fe isotope variations in the modern and ancient Earth and other planetary bodies, in: C.M. Johnson, B.L. Beard, F. Albarede (Eds.), Geochemistry of non-traditional stable isotopes, Reviews in Mineralogy and Geochemistry, vol. 55, Mineralogical Society of America, Washington D.C., 2004, pp. 319–357.
[6] C.M. Johnson, B.L. Beard, E.E. Roden, D.K. Newman, K.H. Nealson, Isotopic constraints on biogeochemical cycling of Fe, in: C.M. Johnson, B.L. Beard, F. Albarede (Eds.), Geochemistry of non-traditional stable isotopes, Reviews in Mineralogy and Geochemistry, vol. 55, Mineralogical Society of America, Washington D.C., 2004, pp. 359–408.
[7] T.D. Bullen, A.F. White, C.W. Childs, D.V. Vivit, M.S. Schulz, Demonstration of significant abiotic iron isotope fractionation in nature, Geology 29 (2001) 699–702.
[8] A.M. Matthews, X.K. Zhu, K. O'Nions, Kinetic iron stable isotope fractionation between iron (II) and iron (III) complexes in solution, Earth Planet. Sci. Lett. 192 (2001) 81–92.
[9] S.A. Welch, B.L. Beard, C.M. Johnson, P.S. Braterman, Kinetic and equilibrium Fe isotope fractionation between aqueous Fe(II) and Fe(III), Geochim. Cosmochim. Acta 67 (2003) 4231–4250.
[10] L.R. Croal, C.M. Johnson, B.L. Beard, D.K. Newman, Iron isotope fractionation by Fe(II)-oxidizing photoautotrophic bacteria, Geochim. Cosmochim. Acta 68 (2004) 1227–1242.
[11] S.L. Brantley, L.J. Liermann, R.L. Guynn, A. Anbar, G.A. Icopini, J. Barling, Fe isotopic fractionation during mineral dissolution with and without bacteria, Geochim. Cosmochim. Acta 68 (2004) 3189–3204.
[12] A.D. Anbar, J.E. Roe, J. Barling, K.H. Nealson, Non-biological fractionation of iron isotopes, Science 288 (2000) 126–128.
[13] J.L. Skulen, B.L. Beard, C.M. Johnson, Kinetic and equilibrium Fe isotope fractionation between aqueous Fe(III) and hematite, Geochim. Cosmochim. Acta 66 (2002) 2995–3015.
[14] R.A. Wiesli, B.L. Beard, C.M. Johnson, Experimental determination of Fe isotope fractionation between aqueous Fe(II), siderite and "green rust" in abiotic systems, Chem. Geol. 211 (2004) 343–362.
[15] O. Rouxel, N. Dobbek, J. Ludden, Y. Fouquet, Iron isotope fractionation during oceanic crust alteration, Chem. Geol. 202 (2003) 155–182.
[16] O. Rouxel, Y. Fouquet, J.N. Ludden, Subsurface processes at the Lucky Strike hydrothermal field, Mid-Atlantic Ridge: evidence from sulfur, selenium, and iron isotopes, Geochim. Cosmochim. Acta 68 (2004) 2295–2311.
[17] B.L. Beard, C.M. Johnson, J.L. Skulan, K.H. Nealson, L. Cox, H. Sun, Application of Fe isotopes to tracing the geochemical and biological cycling of Fe, Chem. Geol. 195 (2003) 87–117.
[18] S. Graham, N. Pearson, S. Jackson, W. Griffin, S.Y. O'Reilly, Tracing Cu and Fe from source to porphyry: in situ determination of Cu and Fe isotope ratios in sulfides from the Grasberg Cu–Au deposit, Chem. Geol. 207 (2004) 147–169.
[19] A.M. Matthews, H.S. Morgans-Bell, S. Emmanuel, H.C. Jenkyns, Y. Erel, L. Halicz, Controls on iron-isotope fractionation in organic-rich sediments (Kimmeridge Clay, Upper Jurassic, Southern England), Geochim. Cosmochim. Acta 68 (2004) 3107–3123.
[20] C.M. Johnson, B.L. Beard, N.J. Beukes, C. Klein, J.M. O'Leary, Ancient geochemical cycling in the Earth as inferred from Fe isotope studies of banded iron formations from the Transvaal Craton, Contrib. Mineral. Petrol. 144 (2003) 523–547.
[21] O.J. Rouxel, A. Bekker, K.J. Edwards, Iron isotope constraints on the Archean and Paleoproterozoic ocean redox state, Science 307 (2005) 1088–1091.
[22] D. Rickard, Kinetics of FeS precipitation: Part 1. Competing reaction mechanisms, Geochim. Cosmochim. Acta 59 (1995) 4367–4379.
[23] A.R. Lennie, S.A.T. Redfern, P.F. Schofield, D.J. Vaughan, Synthesis and Rietveld crystal structure refinement of mackinawite, tetragonal FeS, Min. Mag. 59 (1995) 677–683.
[24] M. Wolthers, S.J. van der Gaast, D. Rickard, A surface and structural model describing the environmental reactivity of disordered mackinawite, Am. Mineral. 88 (2003) 2007–2015.
[25] R.A. Berner, Sedimentary pyrite formation, Am. J. Sci. 268 (1970) 1–23.
[26] D. Rickard, The chemistry of iron sulfide formation at low temperatures, Stockh. Contrib. Geol. 20 (1969) 67–95.
[27] R.E. Sweeney, I.R. Kaplan, Pyrite framboid formation: laboratory synthesis and marine sediments, Econ. Geol. 68 (1973) 618–634.
[28] M.A.A. Schoonen, H.L. Barnes, Reactions forming pyrite and marcasite from solution: II. Via FeS precursors below 100 °C, Geochim. Cosmochim. Acta 60 (1991) 115–134.
[29] R.T. Wilkin, H.L. Barnes, Pyrite formation by reactions of iron monosulfides with dissolved inorganic and organic sulphur species, Geochim. Cosmochim. Acta 60 (1996) 41267–4179.

[30] D. Rickard, Kinetics and mechanism of pyrite formation at low temperatures, Am. J. Sci. 275 (1975) 636–652.
[31] G.W. Luther III, Pyrite synthesis via polysulfide compounds, Geochim. Cosmochim. Acta 55 (1991) 2839–2849.
[32] D. Rickard, Kinetics of pyrite formation by the $H_2S$ oxidation of iron (II) monosulfide in aqueous solutions between 25 °C and 125 °C: the rate equation, Geochim. Cosmochim. Acta 61 (1997) 115–134.
[33] D. Rickard, G.W. Luther III, Kinetics of pyrite formation by the $H_2S$ oxidation of iron (II) monosulfide in aqueous solutions between 25 °C and 125 °C: the mechanism, Geochim. Cosmochim. Acta 61 (1997) 135–147.
[34] I.B. Butler, M.E. Bottcher, D. Rickard, A. Oldroyd. Sulfur isotope partitioning during experimental formation of pyrite via the polysulfide and hydrogen sulfide pathways: implications for the interpretation of sedimentary and hydrothermal pyrite isotope records. Earth Planet. Sci. Lett., 228, 495–509.
[35] S. Theberge, G.W. Luther III, Determination of the electrochemical properties of a soluble aqueous FeS species present in sulfidic solution, Aquat. Geochem. 3 (1997) 191–211.
[36] F. Albarède, B. Beard, Analytical methods for non-traditional isotopes, in: C.M. Johnson, B.L. Beard, F. Albarede (Eds.), Geochemistry of non-traditional stable isotopes, Reviews in Mineralogy and Geochemistry, vol. 55, Mineralogical Society of America, Washington D.C., 2004, pp. 113–152.
[37] C. Archer, D. Vance, Mass discrimination correction in plasma source mass spectrometry: an example using Cu and Zn isotopes, J. Anal. At. Spectrom. 19 (2004) 656–665.
[38] W. Davison, N. Phillips, B.J. Tabner, Soluble iron sulfide species in natural waters: reappraisal of their stoichiometry and stability constants, Aquat. Sci. 61 (1999) 23–43.
[39] M.E. Böttcher, A.M. Smock, H. Cypionka, Sulfur isotope fractionation during experimental precipitation of iron (II) and manganese (II) sulfide at room temperature, Chem. Geol. 146 (1998) 127–134.
[40] J. Hoefs, Stable Isotope Geochemistry, Springer-Verlag, Berlin, Heidelberg, 1997, p. 201.
[41] M. Eigen, R.G. Wilkins, The kinetics and mechanism of formation of metal complexes, Mechanisms of Inorganic Reactions, ACS Symposium Series, vol. 49, 1965, pp. 55–80.
[42] O.M. Suleimenov, T.M. Seward, A spectrophotometric study of hydrogen sulphide ionisation in aqueous solutions to 350 °C, Geochim. Cosmochim. Acta 61 (1997) 5187–5198.
[43] E.A. Schauble, G.R. Rossman, H.P. Taylor, Theoretical estimates of equilibrium Fe-isotope fractionations from vibrational spectroscopy, Geochim. Cosmochim. Acta 65 (2001) 2487–2497.
[44] M. Wolthers, L. Charlet, P.R. van der Linde, D. Rickard, C.H. van der Weijden. Surface chemistry of disordered mackinawite (FeS). Geochim. Cosmochim Acta. (in press).
[45] S. Erlich, I.B. Butler, L. Halicz, D. Rickard, A. Oldroyd, A. Matthews, Experimental study of the copper isotope fractionation between aqueous Cu(II) and covellite, CuS, Chem. Geol. 209 (2004) 259–269.
[46] G.W. Luther III, S.M. Theberge, T.F Rozan, D. Rickard, C.C. Rowlands, A. Oldroyd, Aqueous copper sulfide clusters as intermediates during copper sulfide formation, Environ. Sci. Technol. 36 (2002) 394–402.
[47] I.B. Butler, C. Archer, S. Erlich, D. Vance, A. Matthews, D. Rickard, Transition metal isotope fractionation on sulfide mineral precipitation, Geochim. Cosmochim. Acta 68 (2004) A219.
[48] R.M. Smith, A.E. Martell, Critical Stability Constants, v.4, Inorganic Complexes, Plenum Press, 1976.
[49] D.R. Turner, M. Whitfield, A.G. Dickson, The equilibrium speciation of dissolved components in freshwater and seawater at 25 °C and 1 atm pressure, Geochim. Cosmochim. Acta 45 (1981) 855–881.
[50] D.E. Canfield, R. Raiswell, Pyrite formation and fossil preservation, in: P.A. Allison, D.E.G. Briggs (Eds.), Taphonomy: Releasing the Data Locked in the Fossil Record, Plenum, New York, 1991, pp. 337–387.
[51] D.E. Canfield, R. Raiswell, S.H. Bottrell, The reactivity of sedimentary iron minerals towards sulfide, Am. J. Sci. 292 (1992) 659–683.
[52] B.B. Jorgensen, M.E. Bottcher, H.L. Uschen, L.N. Neretin, I.I. Volkov, Anaerobic methane oxidation and a deep $H_2S$ sink generate isotopically heavy sulfides in Black Sea sediments, Geochim. Cosmochim. Acta 68 (2004) 2095–2118.
[53] L.N. Neretin, M.E. Bottcher, B.B. Jorgensen, I.I. Volkov, H.L. Uschen, K. Hilgenfeld, Pyritization processes and greigite formation in the advancing sulfidization front in the Upper Pleistocene sediments of the Black Sea, Geochim. Cosmochim. Acta 68 (2004) 2081–2093.
[54] V.B. Polyakov, S.D. Mineev, The use of Mössbauer spectroscopy in stable isotope geochemistry, Geochim. Cosmochim. Acta 64 (2000) 849–865.
[55] D. Rickard, Kinetics and mechanisms of the sulfidation of goethite, Am. J. Sci. 274 (1974) 941–952.
[56] A.J. Pyzik, S.E. Sommer, Sedimentary iron monosulfides: kinetics and mechanism of formation, Geochim. Cosmochim. Acta 45 (1981) 687–698.